Supplemental Material for

Natural and anthropogenic geochemical tracers to investigate residence times and groundwater-surface-water interactions in an urban alluvial aquifer

Connor P. Newman*[1], Suzanne S. Paschke[1], Gabrielle Keith[1]

[1] U.S. Geological Survey, Colorado Water Science Center, Denver Federal Center, PO Box 25046, MS-415, Denver, CO, USA, 80225

*cpnewman@usgs.gov

Table of Contents

S1. Introduction

This supplementary material contains additional details on geochemical analyses within the Fountain Creek alluvial aquifer, Colorado. Specifically, details are included pertaining to major-ion and trace-element geochemistry, principal component analysis (PCA), tritium in precipitation, $^{3}H/^{3}He$ apparent ages, groundwater recharge temperature, and groundwater-flow direction. Attributes of all sites where data collection occurred are summarized in Table S1.

Table S1 Attributes of data-collection sites for investigation of the Fountain Creek alluvial aquifer. Data can be accessed from the U.S. Geological Survey National Water Information System (U.S. Geological Survey, 2020) using the site IDs and by selecting the link for 'Field/Lab water-quality samples'.

U.S. Geological Survey Site ID	Site Alias	Location Type	Geographic Grouping	East Coordinates (North American Datum of 1983, Zone 13N, meters)	North Coordinates (North American Datum of 1983, Zone, 13N, meters)
384718104463701	3DAA	Groundwater	Central	519326	4293311

U.S. Geological Survey Site ID	Site Alias	Location Type	Geographic Grouping	East Coordinates (North American Datum of 1983, Zone 13N, meters)	North Coordinates (North American Datum of 1983, Zone, 13N, meters)
384509104435901	CO259-25	Groundwater	Central	523150	4289345
384437104422601	DBA	Groundwater	Central	525398	4288366
384112104421301	FTN1	Groundwater	Central	525770	4282051
384639104461401	BAC1	Groundwater	Central	519884	4292110
384408104424701	NONUM-2	Groundwater	Central	524893	4287470
384617104455901	CAD1	Groundwater	Central	520248	4291433
384648104454501	TH-22	Groundwater	Central	520583	4292389
384534104450302	U-11	Groundwater	Central	521603	4290111
384513104445302	U-12	Groundwater	Central	521846	4289465
384433104440701	U-14B	Groundwater	Central	522960	4288235
384420104432601	U-15	Groundwater	Central	523951	4287837
384604104451502	U-9	Groundwater	Central	521311	4291035
384217104402901	JCC	Groundwater	Central	528283	4284046
384233104425801	A1	Groundwater	Proximal to creek	524683	4284542
384540104453601	TH-46	Groundwater	Proximal to creek	520806	4290294
384503104451601	TH-5	Groundwater	Proximal to creek	521292	4289155
384636104465401	TH-52	Groundwater	Proximal to creek	518919	4292015
384652104465101	U-7	Groundwater	Proximal to creek	518990	4292509
384824104405101	03-002	Groundwater	Tributary alluvium	527719	4295376
384710104431201	04-009	Groundwater	Tributary alluvium	524320	4293088
384719104444701	CO259-26	Groundwater	Tributary alluvium	521980	4293349
384949104424501	MW 1-1	Groundwater	Tributary alluvium	524955	4297973
384848104413901	MW2-4	Groundwater	Tributary alluvium	526541	4296103
384929104431101	T01-MW002	Groundwater	Tributary alluvium	524340	4297363
384956104422801	T02-MW006	Groundwater	Tributary alluvium	525373	4298203
384917104422701	T04-MW004	Groundwater	Tributary alluvium	525403	4296995
384818104415701	T07-MW004	Groundwater	Tributary alluvium	526112	4295174
384758104422301	T07-MW006	Groundwater	Tributary alluvium	525503	4294570
384732104430901	T13-MW004	Groundwater	Tributary alluvium	524377	4293769
384840104481200	CANAL 4 AT HEADGATE	Surface Water	Canal 4	517029	4295833
384610104441700	CANAL 4 DS HANCOCK ROAD	Surface Water	Canal 4	522710	4291224
384458104423000	CANAL 4 NR FTN VAL SCHL	Surface Water	Canal 4	525299	4289013
384720104455400	CANAL 4 DS SAND CREEK	Surface Water	Canal 4	520363	4293375
384531104432200	WINDMILL GULCH @ BRADLEY	Surface Water	Other surface water	524041	4290026

U.S. Geological Survey Site ID	Site Alias	Location Type	Geographic Grouping	East Coordinates (North American Datum of 1983, Zone 13N, meters)	North Coordinates (North American Datum of 1983, Zone, 13N, meters)
07105800	FOUNTAIN CREEK AT SECURITY, CO	Surface Water	Fountain Creek	523133	4286787
383854104413601	FOUNTAIN CR BELOW JIMMY CAMP CR NR FOUNTAIN, CO	Surface Water	Fountain Creek	526695	4277810
07105530	FOUNTAIN CR BLW JANITELL RD BLW COLO. SPRINGS, CO	Surface Water	Fountain Creek	517730	4294941
07105900	JIMMY CAMP CREEK AT FOUNTAIN, CO.	Surface Water	Other surface water	527086	4281806
07105600	SAND CREEK ABOVE MOUTH AT COLORADO SPRINGS, CO	Surface Water	Other surface water	519640	4293312
384833104473900	SPRING CK DS LAS VEGAS ST	Surface Water	Other surface water	517825	4295619

S2. Major Ions and Trace Elements

Analysis of major ions in the alluvial aquifer indicates that waters in different regions of the aquifer display slightly different compositions, as well as apparent differences between surface waters and groundwaters. Surface waters are commonly Na+K-Cl type waters (Fig. S1), possibly indicating the influence of road salt or wastewater effluent on their compositions (Fig. S2). Groundwaters range in composition from predominantly Ca-HCO_3 waters (tributary alluvium) to mixed Ca-Na+K-HCO_3-SO_4 waters in the portions of the aquifer that are central and proximal to creeks (Fig. S1). The central quadratic portion of the Piper diagram indicates that mixing of groundwater in the tributary alluvium and surface waters could explain much of the variability of central and proximal-to-creek groundwaters.

Mixing analyses conducted with Cl/Br ratios and Cl concentrations (Alcalá, and Custodio, 2008; Davis et al., 1998; McArthur et al., 2012) indicate that groundwater in the tributary alluvium is closest to atmospheric Cl/Br ratios and is most dilute in terms of Cl concentration. Well 04-009 has an end-member composition that is interpreted to represent native groundwater recharge in the area. The exception to dilute groundwater in the tributary alluvium is observed in wells 03-002, T01-MW002, T04-MW004, and MW 1-1. Well T04-MW004 is consistent with septic tank discharge, and well MW 1-1 is consistent with addition of road salt. Wells 03-0002 and T01-MW002 have compositions indicating other sources of Cl aside from the end members considered here. Groundwaters in the central zone and proximal to creeks can be explained by variable mixtures of native groundwater recharge and mixing with combinations of septic tank discharge, road salt, and wastewater treatment plant (WWTP) effluent. Well TH-52 (proximal to Fountain Creek) lies nearly perfectly on a mixing line between native groundwater recharge and WWTP effluent. No groundwater compositions are indicative of substantial dissolution of evaporite

minerals in the aquifer. Surface waters also tend to be intermediate between WWTP effluent, road salting, and discharge from septic systems.

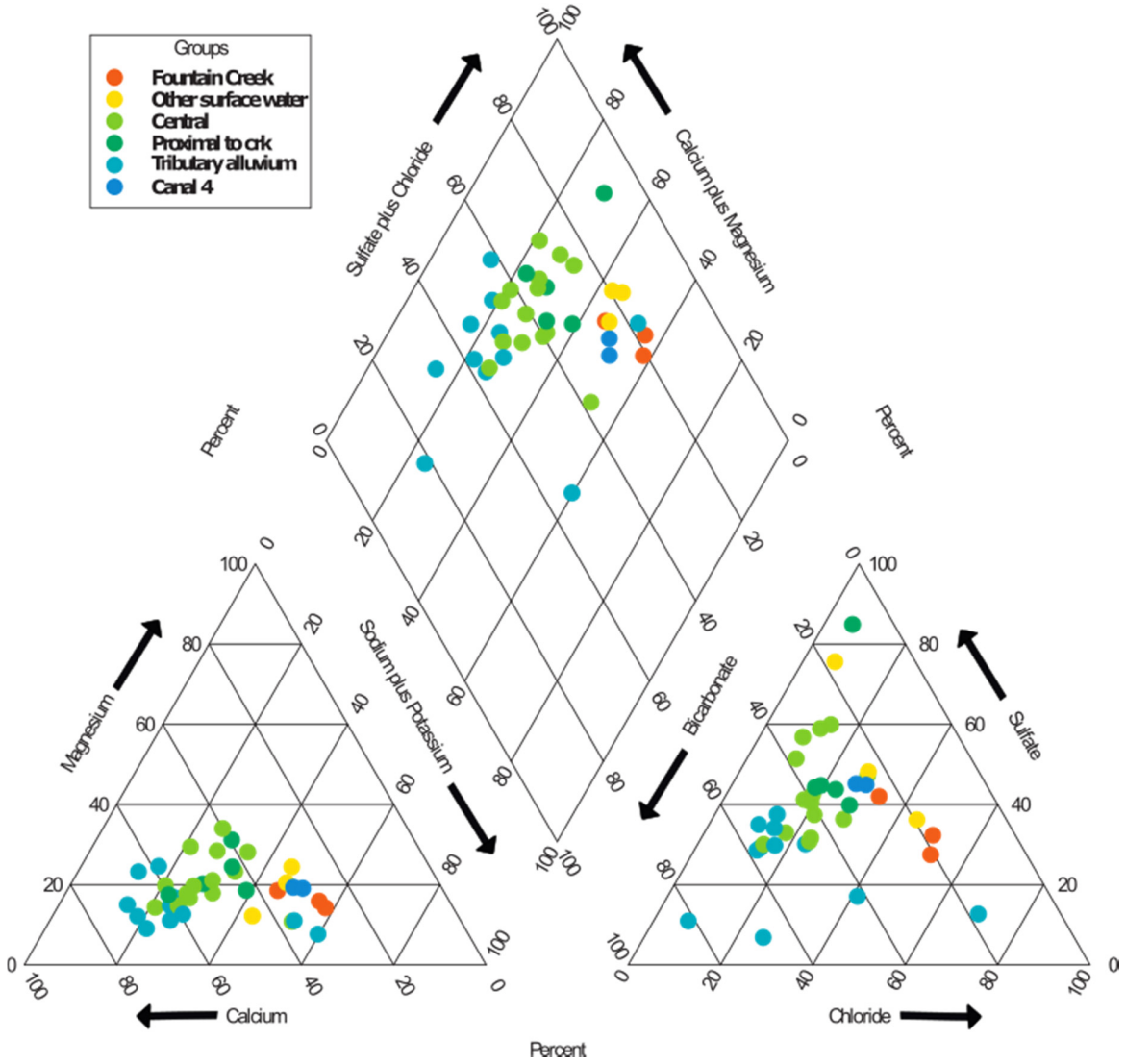

Figure S1 Piper plot (Piper, 1944) displaying variability of major-ion geochemistry of groundwater and surface water in the vicinity of the Fountain Creek alluvial aquifer.

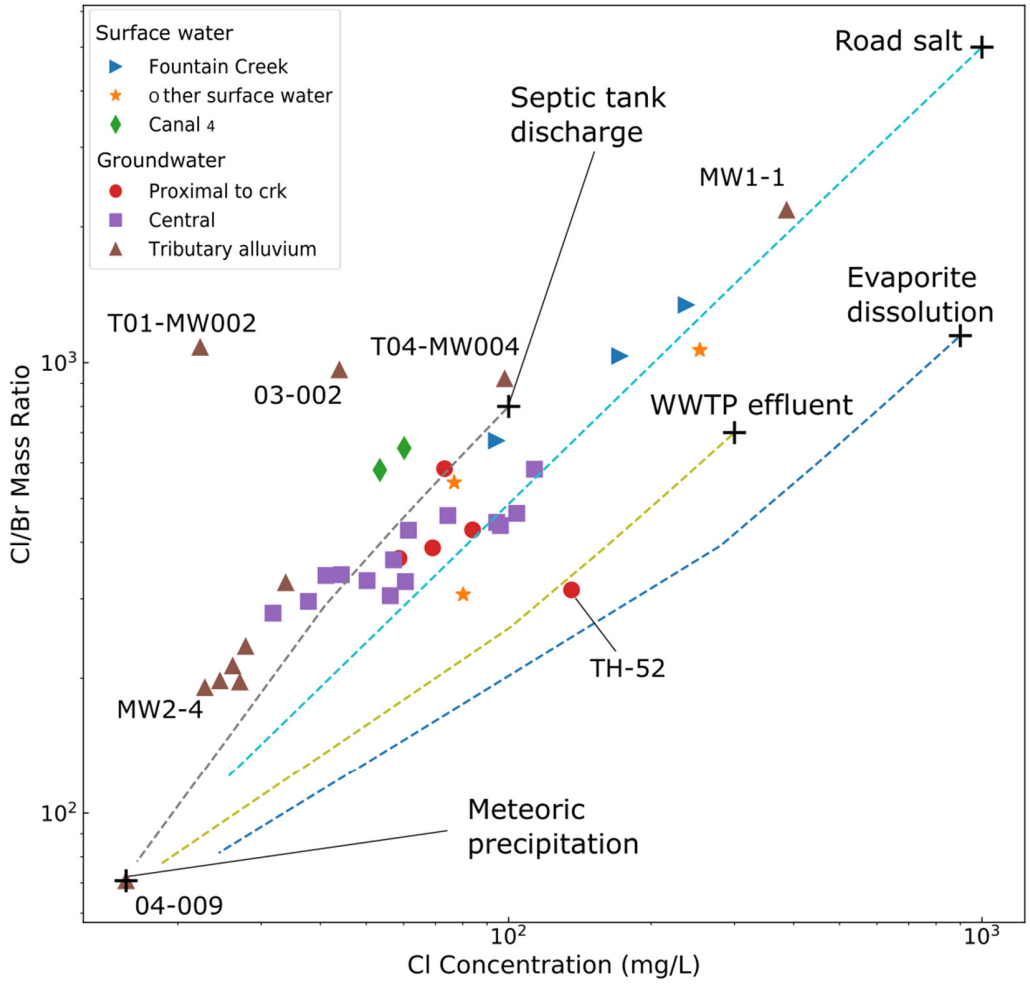

Figure S2 Ratio of Cl/Br (by mass in milligrams per liter [mg/L]) versus Cl concentration for groundwater and surface water, including potential end-member compositions of anthropogenic and geogenic sources (marked with + signs). Mixing lines are displayed between sources and native groundwater for the site, taken as the composition of groundwater from well 04-009 based on its position in mixing space. Specific groundwater wells of interest are noted by the site alias. The end-member compositions of possible sources were estimated from Alcalá and Custodio (2008), Davis et al. (1998), McArthur et al. (2012), and Mullaney et al. (2009).

The redox conditions of groundwater samples were evaluated according to the method of Jurgens et al. (2009) and are displayed in Table S2. Most sites (26 of 31) are classified as oxic whereas the remainder are classified as mixed oxic-anoxic and consistent with reduction of O_2 or Mn^{4+}. It is interesting to note

that none of the sites are classified as being primarily NO_3 reducing, despite isotopic evidence described in the manuscript that indicates NO_3 reduction is likely occurring in some locations. The redox assignment process summarized in Table S2 has a variety of limitations as described by Chapelle et al. (2009), McMahon and Chapelle (2008), and Jurgens et al. (2009). The apparent inconsistency of primary redox conditions is interpreted to be attributable to these various limitations, although it is nonetheless useful for indicating that the Fountain Creek alluvial aquifer is primarily oxic, with some areas of limited reducing conditions.

Table S2 Identification of redox processes in groundwaters of the Fountain Creek alluvial aquifer.

USGS Site ID	Site Alias	Spatial Group	General Redox Category[1]	Redox Process[1]
384233104425801	A1	Proximal to creek	Mixed(oxic-anoxic)	O2-Mn(IV)
384540104453601	TH-46	Proximal to creek	Oxic	O2
384503104451601	TH-5	Proximal to creek	Oxic	O2
384636104465401	TH-52	Proximal to creek	Oxic	O2
384652104465101	U-7	Proximal to creek	Mixed(oxic-anoxic)	O2-Mn(IV)
384824104405101	03-002	Tributary alluvium	Oxic	O2
384710104431201	04-009	Tributary alluvium	Oxic	O2
384719104444701	CO259-26	Tributary alluvium	Oxic	O2
384949104424501	MW 1-1	Tributary alluvium	Oxic	O2
384848104413901	MW2-4	Tributary alluvium	Oxic	O2
384929104431101	T01-MW002	Tributary alluvium	Mixed(oxic-anoxic)	O2-Mn(IV)
384956104422801	T02-MW006	Tributary alluvium	Oxic	O2
384917104422701	T04-MW004	Tributary alluvium	Mixed(oxic-anoxic)	O2-Mn(IV)
384818104415701	T07-MW004	Tributary alluvium	Oxic	O2
384758104422301	T07-MW006	Tributary alluvium	Oxic	O2
384732104430901	T13-MW004	Tributary alluvium	Oxic	O2
384718104463701	3DAA	Central	Oxic	O2
384509104435901	CO259-25	Central	Oxic	O2
384437104422601	DBA	Central	Oxic	O2
384112104421301	FTN1	Central	Oxic	O2
384639104461401	BAC1	Central	Oxic	O2
384408104424701	NONUM-2	Central	Oxic	O2
384617104455901	CAD1	Central	Oxic	O2
384648104454501	TH-22	Central	Oxic	O2
384648104454501	TH-22	Central	Oxic	O2
384534104450302	U-11	Central	Oxic	O2
384513104445302	U-12	Central	Oxic	O2
384433104440701	U-14B	Central	Oxic	O2
384420104432601	U-15	Central	Oxic or Anoxic	O2 or NO3
384604104451502	U-9	Central	Oxic	O2
384217104402901	JCC	Central	Oxic	O2

[1] Redox categories and processes as described by Chapelle et al. (2009), McMahon and Chapelle (2008), and Jurgens et al. (2009).

Calculation of Ce and Eu anomalies allows for further discrimination of redox conditions and geochemical processes in the hydrologic system (Noack et al., 2014). Given that Ce anomalies likely represent redox processes in groundwater (Leybourne and Johannesson, 2008), the anomalies near zero (log [Ce anomaly] values less than zero) are indicative of predominantly oxidizing conditions consistent with analyses using the method of Jurgens et al. (2009). Greater Ce anomalies in surface water are likely due to a complex mix of processes (Leybourne and Johannesson, 2008). Contrastingly Eu anomalies are likely inherited from geochemical interactions with the aquifer matrix (Göb et al., 2013) whereas surface-water Eu anomalies are linked to anthropogenic influx of Gd (North American Shale Composite normalized Gd concentrations are used in calculation of Eu anomaly). Spatial distributions of Gd and Eu anomalies (Fig. S4) illustrate the spatial variability in both groundwater and surface water.

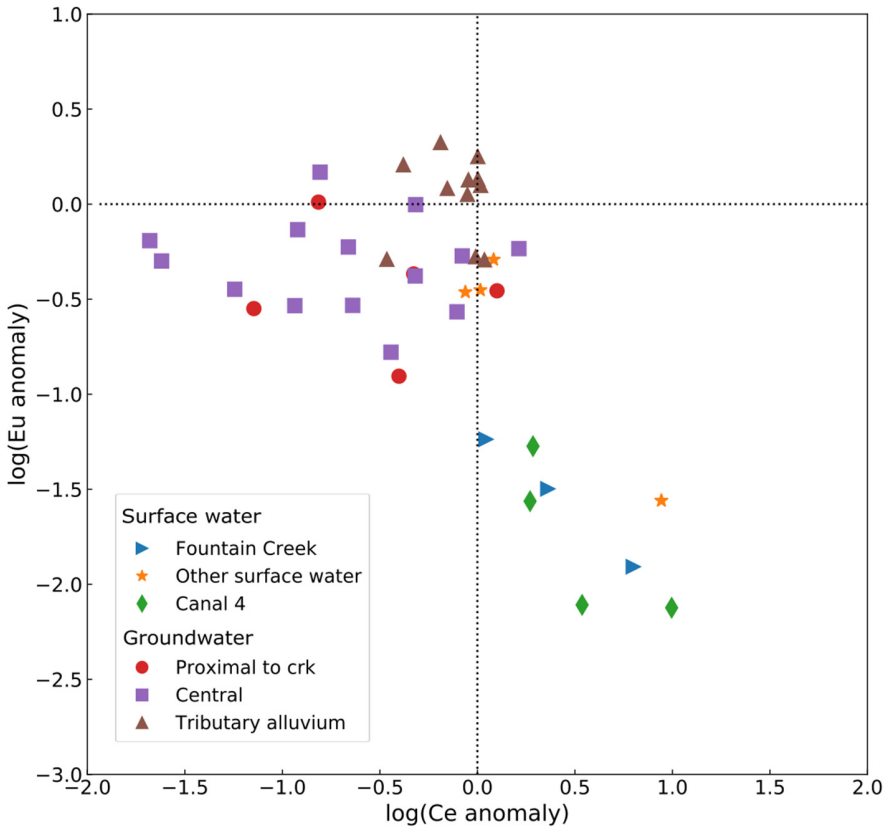

Figure S3 Plot of log(Ce anomaly) versus log(Eu anomaly) in the Fountain Creek alluvial aquifer and adjacent surface waters.

A variety of constituents have been shown by previous research (Mau et al., 2007) to be sourced from anthropogenic activities in the area, including Al, Cu, Fe, Mn, Pb, and Zn. Spatial distributions of these constituents in groundwaters and surface waters (Fig. S5) indicate that different processes affect their transport, or that different sources are present for these metals.

Spatial analysis of constituents of emerging concern (CECs) in surface water and groundwater indicate differing distributions of constituents (Fig. S6). Several CECs may be sourced from different locations or have variable residence times in the environment.

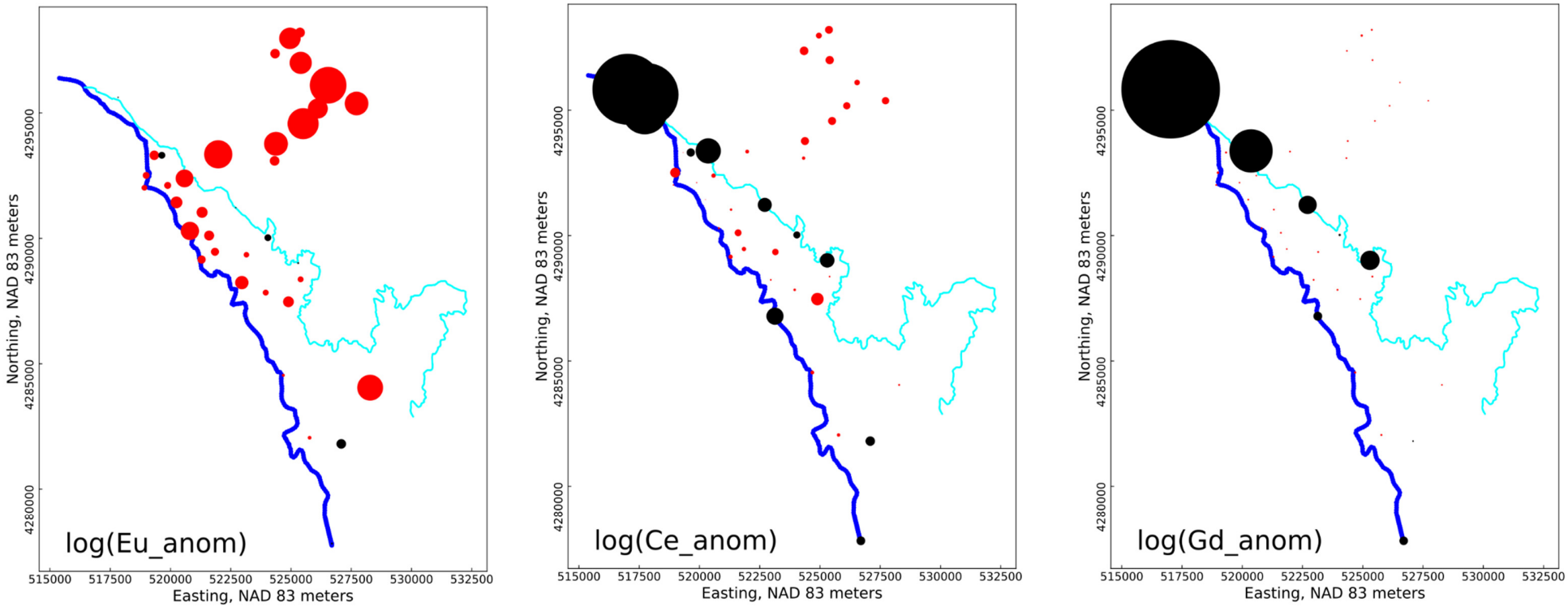

Figure S4 Maps of logarithms of rare earth element (REE) anomalies in groundwater and surface waters associated with the Fountain Creek alluvial aquifer. Symbol sizes are not linked to absolute anomaly value but are representative of the range of values of a given anomaly scaled according to deviations from the median of the anomaly. Groundwater wells are shown in red circles and surface-water locations are shown in black circles. The dark blue line illustrates the path of Fountain Creek and the light blue line illustrates the path of Canal 4. Coordinates are in the North American Datum of 1983 (NAD83), meters.

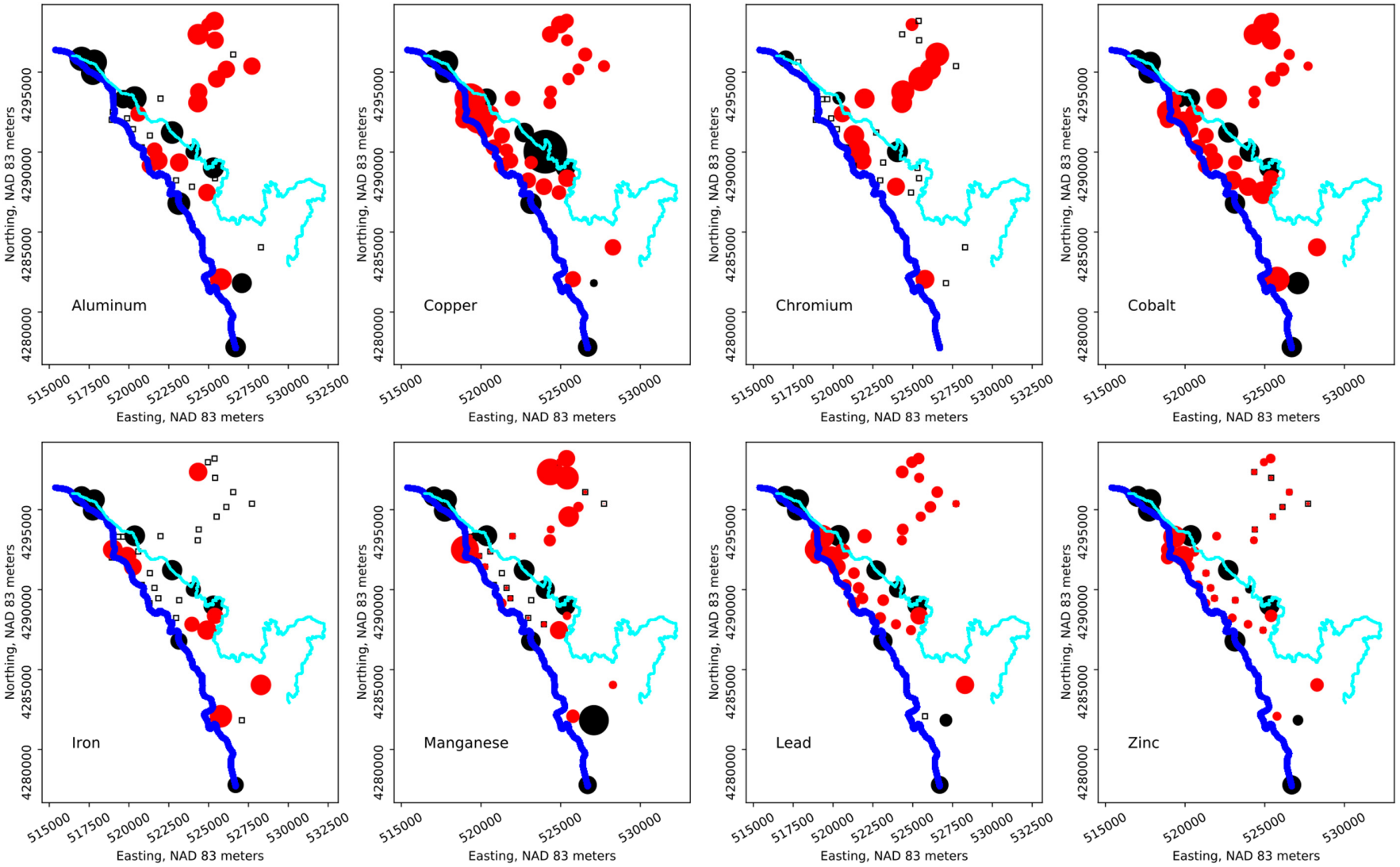

Figure S5 Maps of trace-metal concentrations in groundwater and surface waters associated with the Fountain Creek alluvial aquifer. Symbol sizes are not linked to absolute concentration but are representative of the range of concentrations of a given solute scaled according to deviations from the median concentration of that solute. Open square symbols represent monitoring locations where the constituent of interest was less than the laboratory reporting limit, groundwater wells are shown in red circles, and surface-water locations are shown in black circles. The dark blue line illustrates the path of Fountain Creek and the light blue line illustrates the path of Canal 4. Coordinates are in the North American Datum of 1983 (NAD83), meters.

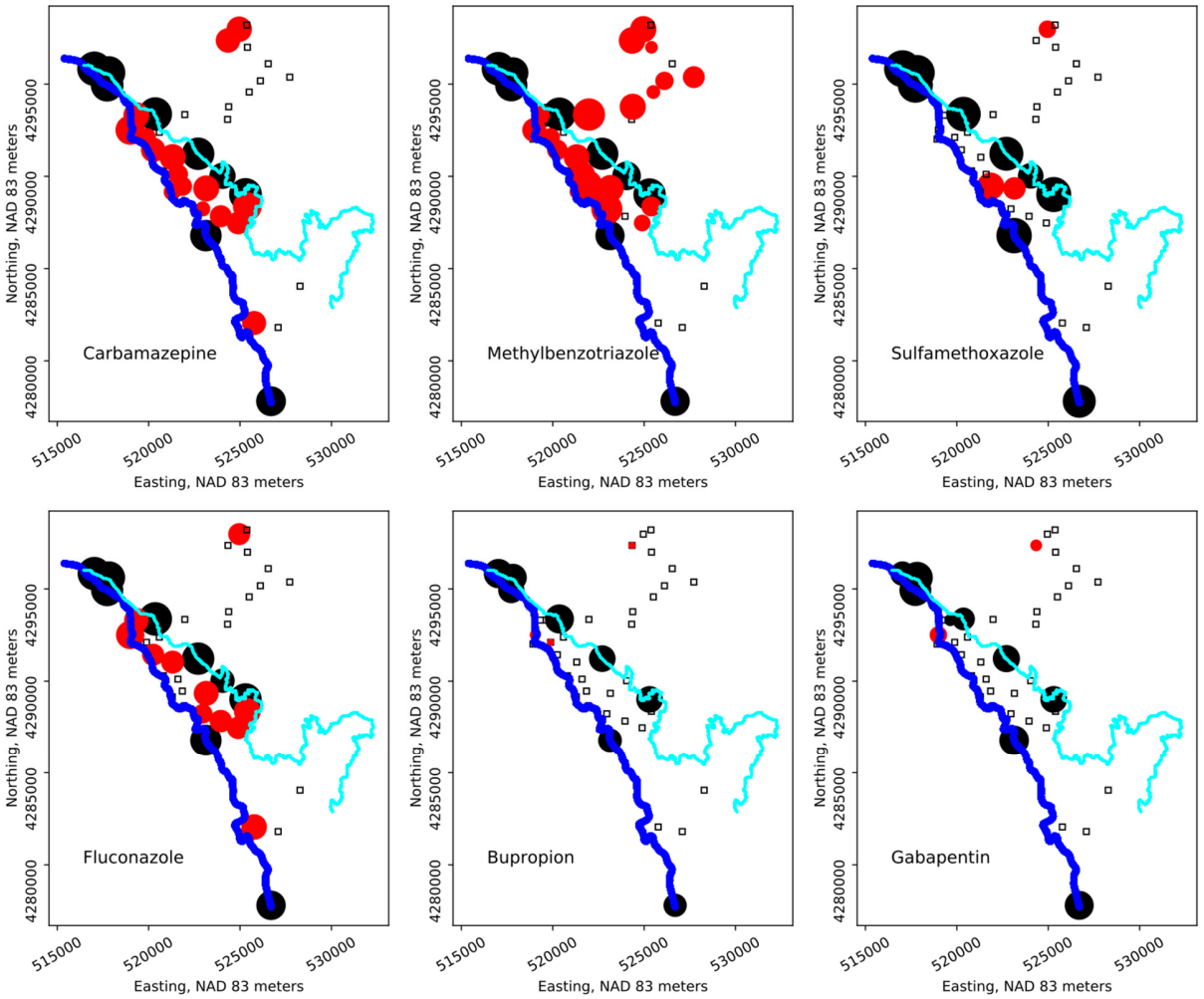

Figure S6 Maps of wastewater indicator compounds and pharmaceutical concentrations in groundwater and surface waters associated with the Fountain Creek alluvial aquifer. Symbol sizes are not linked to absolute concentration but are representative of the range of concentrations of a given solute scaled according to deviations from the median concentration of the given solute. Open square symbols represent monitoring locations where the constituent of interest was less than the laboratory reporting limit, groundwater wells are shown in red circles, and surface-water locations are shown in black circles. The dark blue line illustrates the path of Fountain Creek and the light blue line illustrates the path of Canal 4. Coordinates are in the North American Datum of 1983 (NAD83), meters.

S3. Principal Component Analysis

Principal components analysis (PCA) was conducted first for each sub-grouping of water-quality parameter types (noble gases, trace elements, REE, etc.), then on a subset of parameters determined to be of interest. Figs. S7, S8, and S9 illustrate results of REE-, trace metal-, and noble-gas isotope-specific PCA.

Results of REE-specific PCA (Fig. S7) illustrate that the majority of surface waters plot near the Gd ray, consistent with prominent Gd anomaly in many surface-water samples. Groundwaters in proximity to the creeks generally plot in the upper portion of the plot in the vicinity of the Eu ray. Tributary alluvium groundwaters and central groundwaters only overlap with one another in a small portion of the plot in the vicinity of the Ce ray.

Results of trace element-specific PCA (Fig. S8) again illustrate little overlap of tributary alluvium groundwaters and central groundwaters, which in this instance show some overlap in the vicinity of the rays for Ni, Ba, Li, and Sr. As in analysis of REE-specific PCA, surface-water samples tend to group near one another between the Mn and Cd rays, both of which were noted by Mau et al. (2007) as being sourced from within the watershed during stormflow.

Results of noble-gas isotope PCA (Fig. S9) illustrate that the gases of different likely origin plot on rays in separate fields of the rotation space. Ne, Ar, and Kr, all of which have isotopic compositions primarily derived from the atmosphere (if radiogenic Ar can be ignored; Aeschbach-Hertig and Solomon, 2013; Porcelli and Ballantine, 2002), plot in the lower right section. Evaluation of the ratio of $^{36}Ar/^{40}Ar$ in samples versus that in the air ($^{36}Ar_{air}/^{40}Ar_{air} = 0.003378$; Aeschbach-Hertig and Solomon, 2013) indicates that sub-surface radiogenic production of ^{40}Ar can be ignored (the average $^{36}Ar_{sample}/^{40}Ar_{sample}$ / $^{36}Ar_{air}/^{40}Ar_{air} = 0.998$). In contrast to these three noble-gas isotope compositions, the He and Xe isotopes plot alone in separate parts of the graph. The isotopic compositions of these two gases are likely being modified by subsurface processes. The He isotope compositions are likely being affected by both tritiogenic and terrigenic ^{3}He production (Mahara et al., 2014). The Xe isotope compositions may be affected by leakage from the underlying Pierre Shale (McMahon et al., 2019). In terms of sample position relative to the rays, most groundwaters plot in a relatively narrow range of values on PC2 but a wide range on PC1 (which explains nearly 93% of the variance). Most variability is aligned with the He, Ar, Ne, and Kr rays, and the linear nature of the points indicates a possible boundary effect (Bern et al., 2019). It would be expected that groundwaters with the longest residence times (central groundwaters) would be located proximal to the terrigenic component He, and that waters more recently recharged (groundwaters in the tributary alluvium and proximal to the creek) would be more proximal to atmospheric components Ar, Ne, and Kr. The opposite behavior is observed however. Taken as a whole, these results indicate that PCA of noble-gas isotopes may have some utility, but would require careful interpretation.

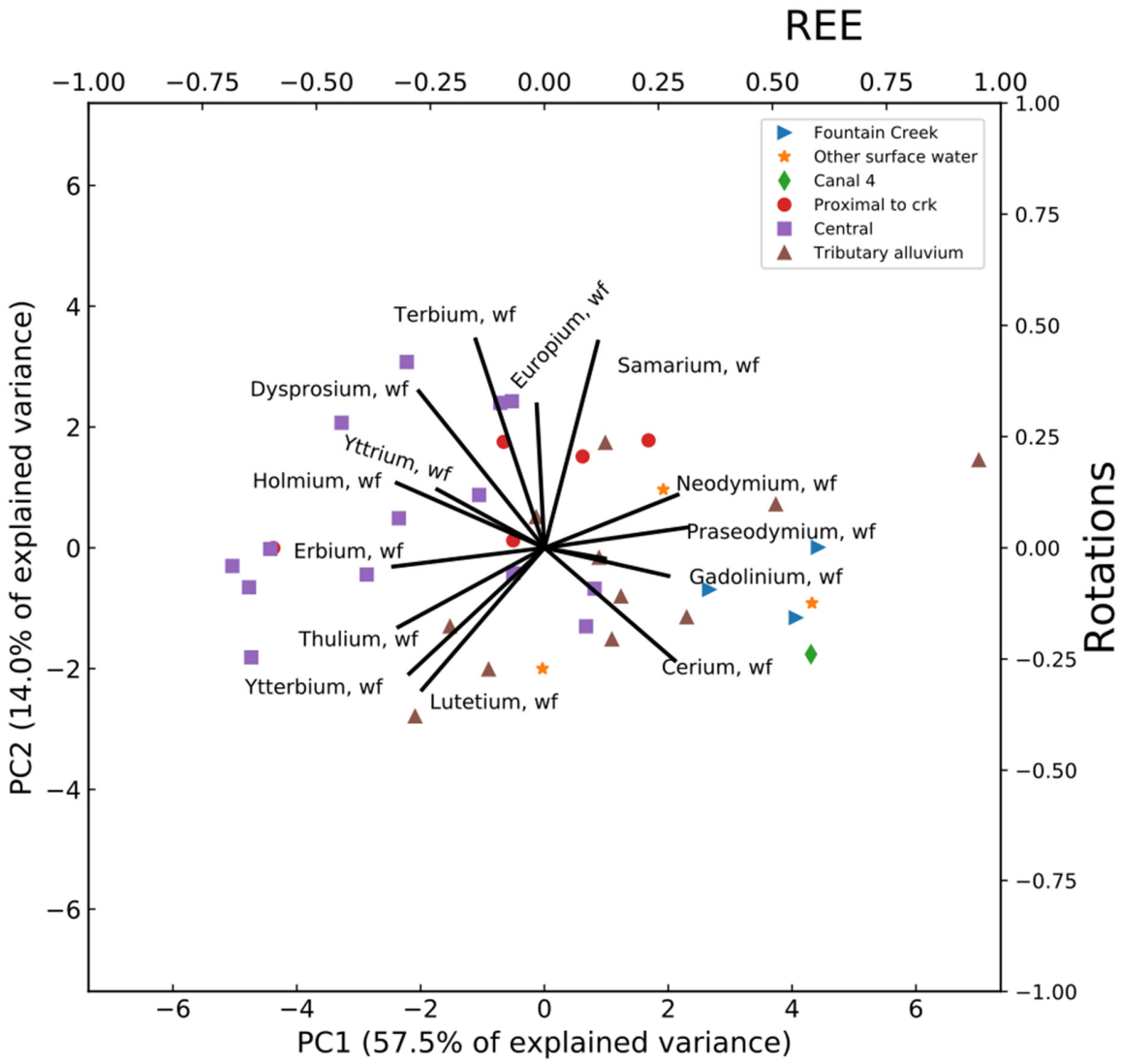

Figure S7 Principal components analysis of rare earth elements. The abbreviation 'wf' indicates that samples were filtered in the field. Rays are plotted against rotations (top and right axes) whereas sample results are plotted against principal component loadings (bottom and left axes).

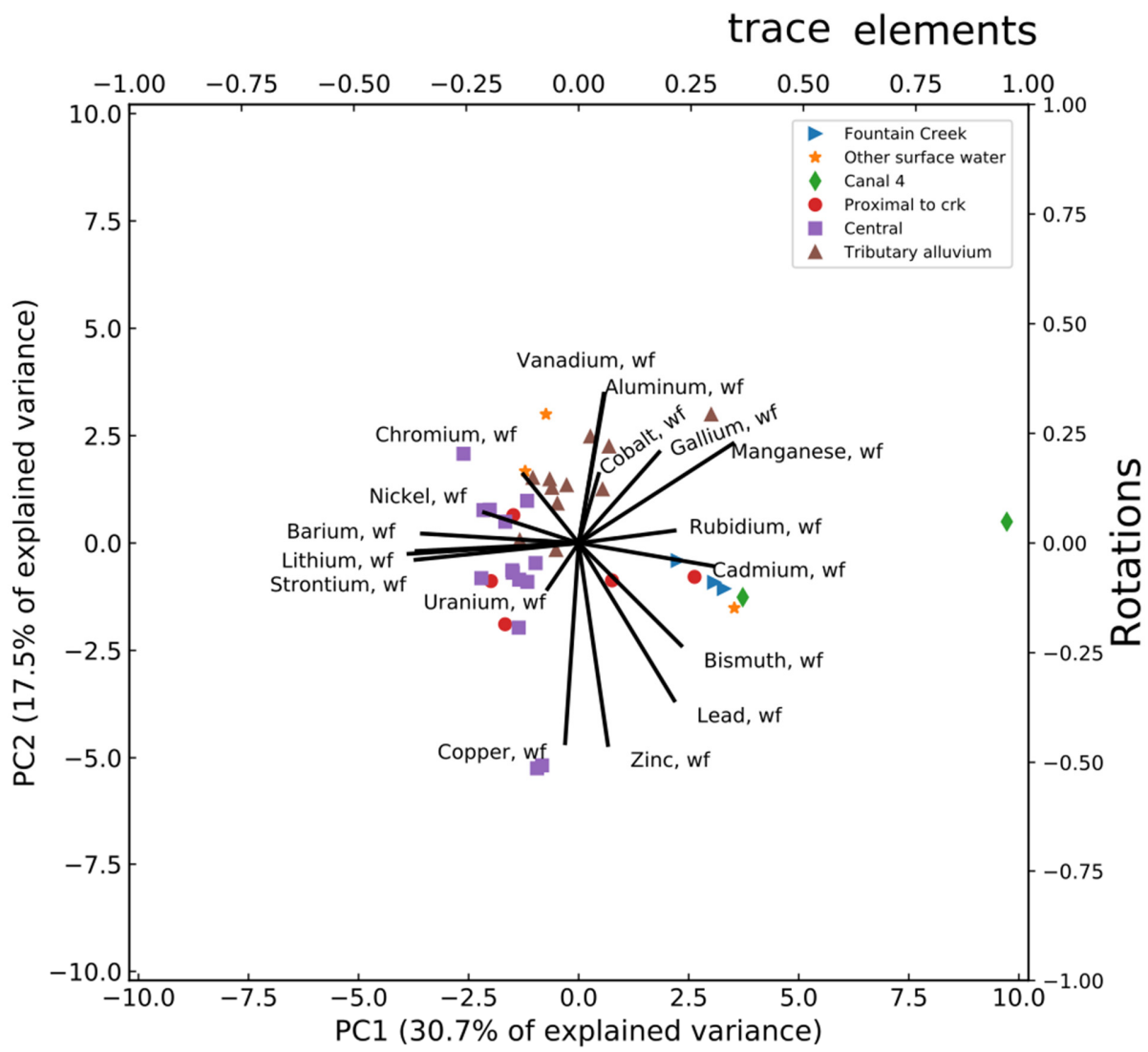

Figure S8 Principal components analysis of trace elements. The abbreviation 'wf' indicates that samples were filtered in the field. Rays are plotted against rotations (top and right axes) whereas sample results are plotted against principal component loadings (bottom and left axes).

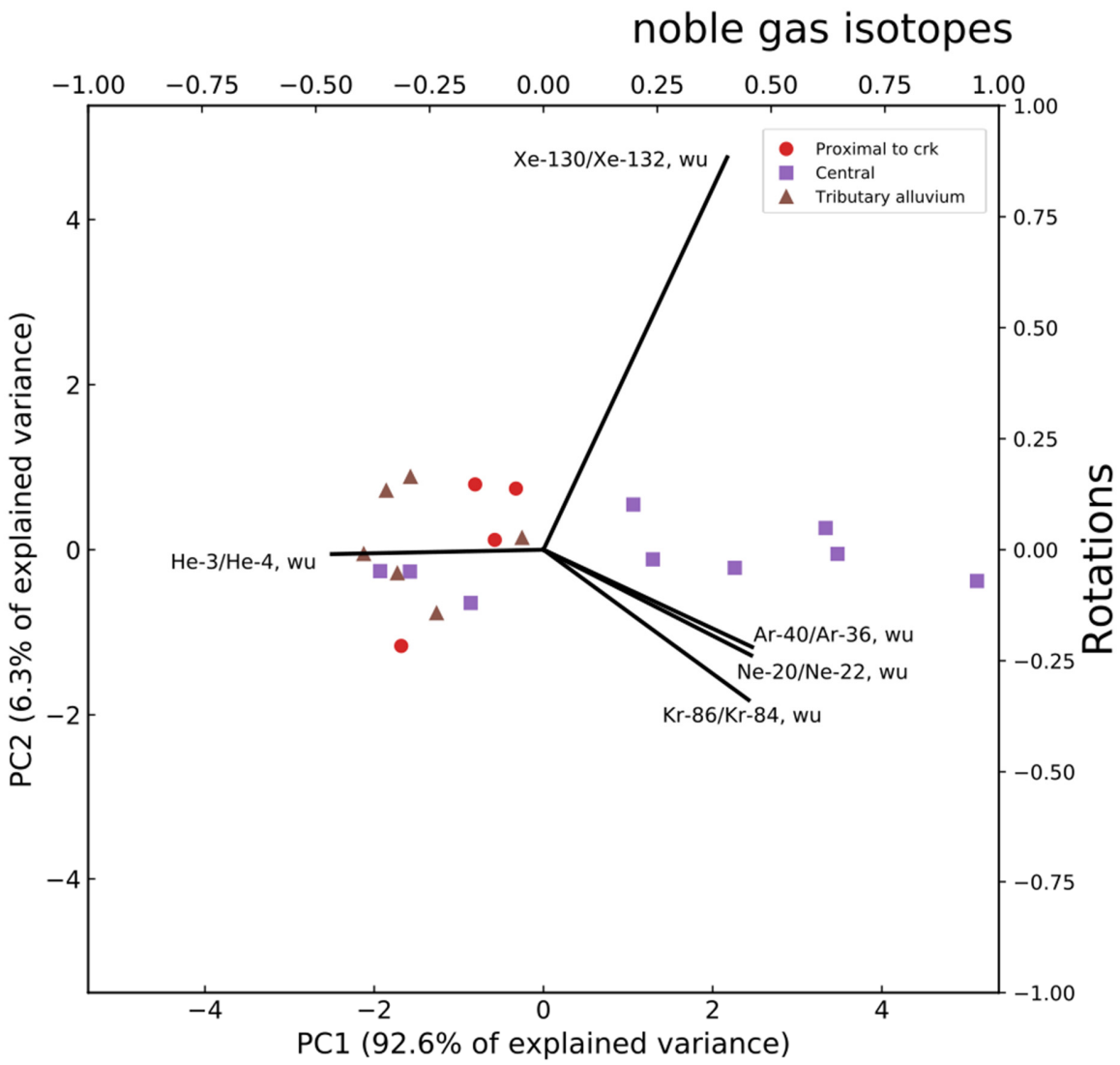

Figure S9 Principal components analysis of noble gas isotopes. The abbreviation 'wu' indicates that samples were not filtered in the field. Rays are plotted against rotations (top and right axes) whereas sample results are plotted against principal component loadings (bottom and left axes).

S4. Tritium in Precipitation

Estimates of tritium in precipitation are available from Jurgens (2018) and Jasechko and Taylor (2015). No published literature has yet evaluated the similarities or differences from using these datasets. Thus, both datasets were compared for the vicinity of the study site to evaluate any discrepancies between the use of such data for calculation of the fraction of young water as based on the fraction of water recharged since the advent of atmospheric nuclear testing in 1953 ($F_{post\text{-}1953}$; Jasechko, 2016).

Jurgens (2018) provides monthly interpolations of tritium in precipitation for rectilinear grids within the continental United States, as described by Michel et al. (2018). Jasechko and Taylor (2015) provide annual interpolated tritium in precipitation for specific coordinates. For use in this analysis, the closest datasets to the Fountain Creek alluvial aquifer, located within El Paso County, Colorado, were selected from Jurgens (2018) and Jasechko and Taylor (2015). The study lies near several intersections of the rectilinear grids of Jurgens (2018), see Fig. S10. Because tritium in precipitation shows a greater north-south gradient than east-west gradient (Michel et al., 2018), two grids were selected. It is assumed that selecting grids to the west of the study area would not substantially change results. For extraction of interpolated values from Jasechko and Taylor (2015), four locations in proximity to the study site were selected (Fig. S10).

Intra-dataset comparison of interpolated tritium in precipitation from the two datasets (Fig. S11) illustrates that the two interpolations derived by Jurgens (2018) are relatively similar, although some interannual differences occur, which are likely attributable to large-scale processes governing tritium deposition (Michel et al., 2018). Interpolated tritium in precipitation from four locations by Jasechko and Taylor (2015) show little variability and are all comparable to one another.

In contrast to intra-dataset comparison, when comparing the interpolations of Jurgens (2018) to Jasechko and Taylor (2015), several important differences are noted. First, interpolated tritium in precipitation from Jasechko and Taylor (2015) starts at a lesser value than from Jurgens, and lacks short-term temporal fluctuations presumably related to individual nuclear tests (see time period in late 1954 on Fig. S11). Second, interpolated tritium in precipitation during the late 1980s/early 1990s is quite different between the two datasets with greater values predicted by Jasechko and Taylor (2015) than Jurgens (2018). Finally, interpolated tritium in precipitation after the year 2009 is also substantially different, but with the opposite relationship as observed in the 1980s/1990s.

The effects of these differences on groundwater recharge and age calculations could be important for several reasons. First, if groundwater were recharged in either of the periods of disagreement (1980s/1990s or 2009-present), then the calculated fractions of young and old water (Jasechko, 2016; Lindsey et al., 2019) would be substantially different. Second, because standard methods of groundwater age formulation use mean or minimum values of decayed tritium in precipitation (Jasechko, 2016; Lindsey et al., 2019), any skew in the dataset has the potential to change apparent groundwater ages.

For use in this research, the interpolated tritium in precipitation dataset of Jurgens (2018) was used because this dataset has monthly resolution and is consistent with the most recent advances in understanding of tritium in precipitation throughout the continental United States.

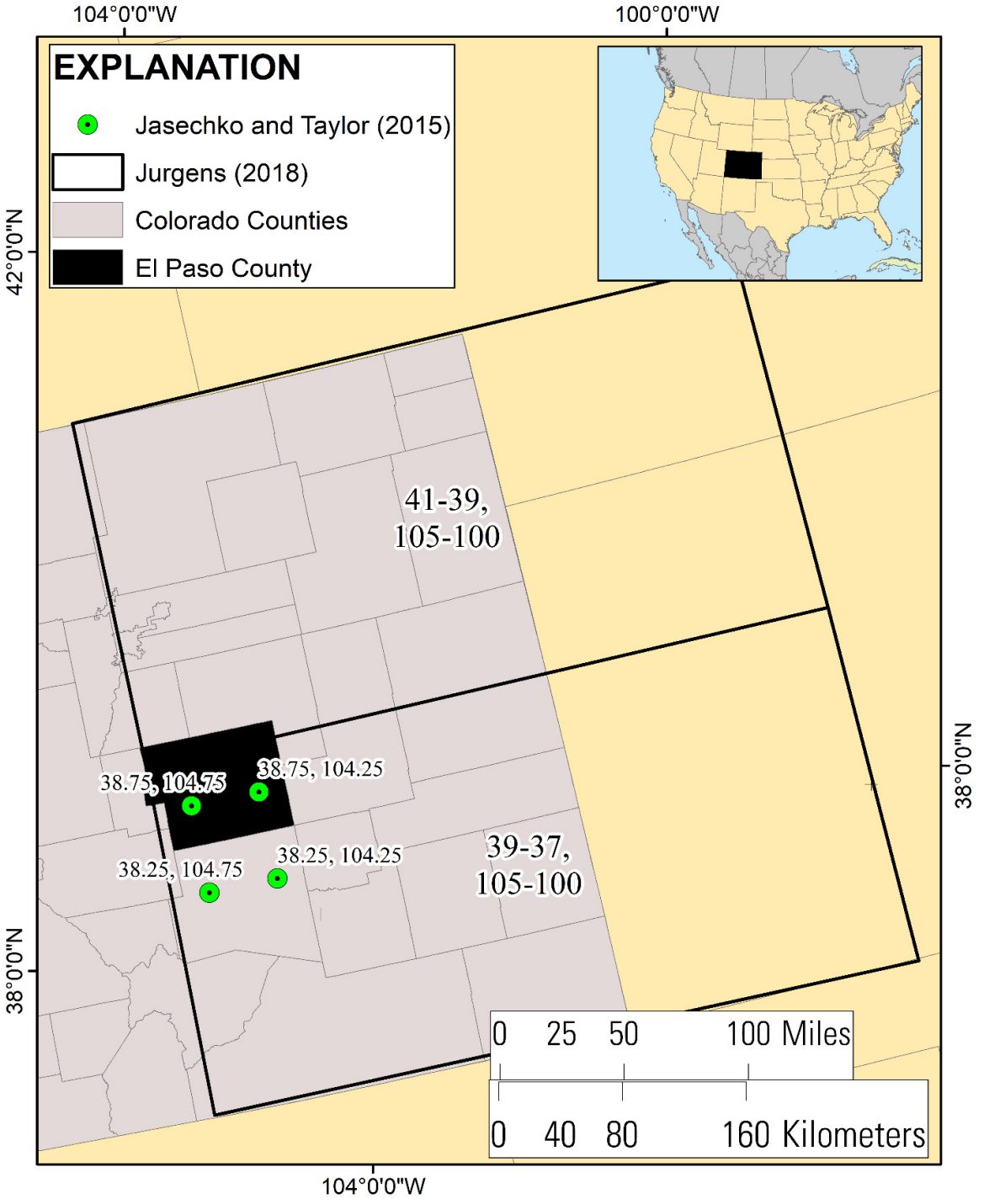

Figure S10 Map of locations for sources of interpolated tritium in precipitation in relation to El Paso County, Colorado. For the data of Jasechko and Taylor (2015)the numbers next to the sample dots represent the latitude and longitude of the locations, and for the quadrangles of Jurgens (2018) the numbers represent the range in latitude and longitude of each quadrangle.

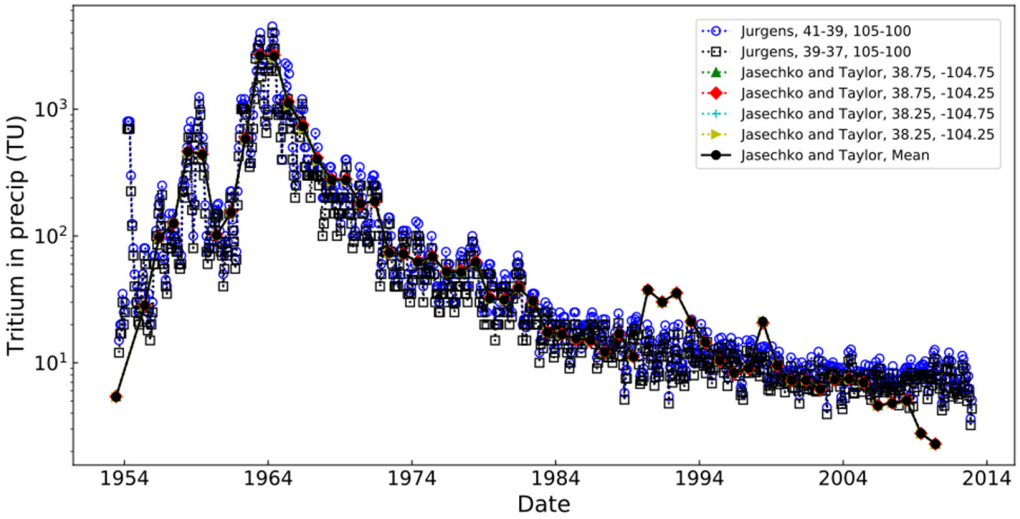

Figure S11 Interpolated tritium in precipitation from Jurgens (2018) for quadrangles (1) 41° N to 39° N, 105° W to 100° W and (2) 39° N to 37° N, 105° W to 100° W, and from Jasechko and Taylor (2015) for locations (1) 38.75° N, 104.75° W, (2) 38.75° N, 104.25° W, (3) 38.25° N, 104.75° W, (4) 38.25° N, 104.25° W, and (5) mean of previous four station values.

S5. $^3H/^3He$ Apparent Age

Kulongoski et al. (2008) provide a method by which a site-specific ratio of $^3He/^4He$ may be calculated. As described in the manuscript, this method was applied to data from the Fountain Creek alluvial aquifer to evaluate sensitivity in apparent $^3H/^3He$ ages. Apparent ages using both the published $^3He/^4He$ for terrigenic He components of 2 x 10^{-8} (Mahara et al., 2014) and site-specific $^3He/^4He$ computed using the method of Kulongoski et al. (2008) are summarized in Table S3.

Table S3 Results of apparent-age calculations using different $^3He/^4He$ ratios to represent terrigenic components

Site Alias	$^3H/^3He$ Apparent Age (years)	
	Standard $^3He/^4He$ Ratio ($R=2*10^{-8}$)	**Site-Specific $^3He/^4He$ Ratio ($R_c=7.11*10^{-7}$)**
04-009	0.0	0.0
A1	0.0	0.0
CO259-25	10.8	0.0
CO259-26	1.2	0.6
FTN1	1.1	0.7
MW 1-1	0.0	0.0
MW2-4	4.9	4.0
NONUM-2	2.7	2.4
CAD1	3.2	0.0

Site Alias	$^3H/^3He$ Apparent Age (years)	
	Standard $^3He/^4He$ Ratio ($R=2*10^{-8}$)	Site-Specific $^3He/^4He$ Ratio ($R_c=7.11*10^{-7}$)
T13-MW004	3.2	1.2
TH-22	1.1	0.0
TH-5	0.6	0.6
TH-52	0.7	0.1
U-12	5.6	0.0
U-14B	6.9	0.0
U-15	0.6	0.0
U-7	0.0	0.0
JCC	21.5	4.9

R = ratio of $^3He/^4He$ attributed to terrigenic He components from crustal interaction (Mahara et al., 2014)

R_c = site specific ratio of $^3He/^4He$ corrected for air-bubble entrainment calculated according to Kulongoski et al. (2008)

These results illustrate that variable apparent ages could be calculated depending on the assumptions used in the calculations and the accuracy of the site-specific He-mass balance. Results using the site-specific R_c appear to be biased young and are inconsistent with piston-flow analysis of SF_6 data and with lumped parameter modeling. Therefore, in this instance, it appears that although He-isotope evolution is occurring in the aquifer, use of the standard He ratio in apparent-age calculations yields results that are more comparable with other data for the study area. Other users of the method described in Kulongoski et al. (2008) would benefit by considering these results when applying the methodology.

S6. Groundwater Recharge Characteristics

Groundwater recharge characteristics, excess air and temperature, were computed using dissolved gases O_2, N_2 (corrected for excess gas), Ar, and CO_2, and using noble gases (where available). Results are summarized in Table S3. Noble-gas modeling was conducted using an inverse approach similar to that described by Peeters et al. (2002). Results of both types of dissolved-gas modeling (major gases and noble gases) is summarized in Table S4.

Sensitivity analyses were conducted to evaluate the response of gas modeling results to changes in the input elevation. To test sensitivity, two different recharge elevations were used in calculations: the maximum elevation within the watershed (2,012 meters above the North American Vertical Datum of 1988 [NAVD88]) and the median between the maximum watershed elevation and the wellhead elevation. Results are summarized in Table S5.

Results indicate that elevation differences could account for up to 2 °C difference in recharge temperature. This difference is consistent with differences that can be caused by application of different models or by modeling method (i.e., if Monte Carlo analyses are included or not; Cey et al., 2009; Jung and Aeschbach, 2018; Sun et al., 2010). Generally, discrepancies are such that base-case recharge temperatures are warmer than sensitivity analyses, but several show the opposite behavior. Overall, the results show that substantial changes are unlikely to occur between recharge elevation, and that the base-case simulations are suitable for the environmental tracer analysis.

Table S4 Results of dissolved gas modeling

Site Alias	Sample Collection Date	Field Temperature (°C)	Excess N (mg/L)	Interpretation Based on Major Gases		Noble Gas Data Available	Interpretation Based on Noble Gases				
				Recharge temperature (°C)	Excess Air (ccSTP/L)		Recharge temperature (°C)	Excess Air (ccSTP/L)	Model	χ^2	Probability (%)
03-002	12/17/2018	15.8	--	17.8	1.47	Yes	9.4	1.27E-04	Partial re-equilibration (PR)	0.966	33%
04-009	12/19/2018	14.3	--	14.4	1.94	Yes	12.6	2.03E+00	Partial re-equilibration (PR)	0.297	96%
A1	3/19/2019	9.2	2	16.5	3.18	Yes	9.7	1.32E-04	Partial re-equilibration (PR)	2.746	10%
3DAA	11/28/2018	12.5	--	16.7	1.46	No	--	--	--	--	--
CO259-25	3/20/2019	14.2	--	13.1	3.38	Yes	11.2	3.68E+00	Partial re-equilibration (PR)	0.099	95%
CO259-26	11/20/2018	14.0	--	12.9	0.63	Yes	11.8	2.09E-01	Partial re-equilibration (PR)	0.103	95%
FTN1	12/6/2018	15.3	--	16.0	2.52	Yes	9.7	1.02E-04	Partial re-equilibration (PR)	2.003	16%
BAC1	11/21/2018	13.5	--	9.0	2.12	No	--	--	--	--	--
MW1-1	12/12/2018	14.5	--	15.2	3.35	Yes	10.4	8.56E-01	Partial re-equilibration (PR)	0.374	83%
MW2-4	12/12/2018	14.7	--	12.7	1.77	Yes	11.5	6.95E+00	Closed-system equilibration (CE)	0.389	94%
NONUM-2	11/30/2018	12.8	--	9.6	3.30	Yes	8.3	4.53E+00	Partial re-equilibration (PR)	0.480	79%
CAD1	11/27/2018	13.7	--	17.1	5.06	Yes	12.6	5.26E+00	Partial re-equilibration (PR)	0.399	53%
T01-MW002	12/13/2018	15.1	1	13.6	3.89	No	--	--	--	--	--
T04-MW004	12/14/2018	14.7	3	13.8	3.37	No	--	--	--	--	--
T07-MW004	12/13/2018	13.3	--	13.1	4.21	No	--	--	--	--	--
T07-MW006	12/18/2018	14.7	--	11.1	3.55	No	--	--	--	--	--
T13-MW004	12/18/2018	14.4	--	12.0	3.07	Yes	9.5	1.95E+00	Partial re-equilibration (PR)	0.000	100%
TH-22	11/19/2018	15.6	--	13.8	1.36	Yes	11.5	1.46E-01	Partial re-equilibration (PR)	0.522	77%

Site Alias	Sample Collection Date	Field Temperature (°C)	Excess N (mg/L)	Interpretation Based on Major Gases		Noble Gas Data Available	Interpretation Based on Noble Gases				
				Recharge temperature (°C)	Excess Air (ccSTP/L)		Recharge temperature (°C)	Excess Air (ccSTP/L)	Model	χ^2	Probability (%)
TH-46	11/28/2018	13.9	--	15.2	2.23	No	--	--	--	--	--
TH-5	12/7/2018	13.1	--	9.3	2.46	Yes	4.3	1.11E-04	Partial re-equilibration (PR)	3.531	6%
TH-52	11/20/2018	16.0	--	17.1	0.48	Yes	--	--	Model Fail	--	--
U-11	12/3/2018	14.3	--	16.4	3.78	No	--	--	--	--	--
U-12	12/10/2018	15.0	--	11.7	2.57	Yes	11.3	3.76E+00	Partial re-equilibration (PR)	0.000	100%
U-14B	11/29/2018	15.6	2	12.6	3.45	Yes	12.4	8.73E+00	Closed-system equilibration (CE)	0.439	93%
U-15	12/4/2018	15.2	--	15.6	0.76	Yes	12.7	4.96E-05	Partial re-equilibration (PR)	1.352	24%
U-7	11/26/2018	15.8	2.5	17.9	3.14	Yes	13.2	2.45E+00	Partial re-equilibration (PR)	1.418	49%
U-9	11/27/2018	14.4	--	15.2	3.55	No	--	--	--	--	--
JCC	3/19/2019	11.9	--	14.0	3.41	Yes	11.4	3.14E+00	Partial re-equilibration (PR)	0.154	93%

Table S5 Sensitivity analysis of recharge temperature to recharge elevation used in noble-gas modeling

Site Alias	Base-Case Noble-Gas Recharge Temperature (°C)[1]	Median Elevation Recharge Temperature (°C)[2]	Maximum Elevation Recharge Temperature (°C)[3]	Average of Sensitivity Estimates of Recharge Temperature (°C)	Difference Between Recharge Temperature Estimates (°C)[4]
TH-5	4.29	5.03	4.55	4.79	0.51
JCC	11.35	9.46	8.93	9.19	-2.16
CAD1	12.64	10.71	10.23	10.47	-2.17
04-009	12.61	11.35	11.01	11.18	-1.44
03-002	9.36	10.51	10.27	10.39	1.03

[1] Base-case noble-gas recharge temperature as summarized in Table S3, with recharge elevation computed using the elevation at the wellhead (the minimum possible elevation of recharge)

[2]Median elevation recharge temperature was computed by calculating the median between the wellhead elevation and the maximum elevation within the watershed

[3]Maximum elevation recharge temperature was computed assuming the recharge elevation equals the maximum elevation within the watershed (2,012 meters above NAVD88)

[4]Computed as $R_{T-avg\ Sens.} - R_{T-BC}$ where: $R_{T\text{-avg Sens.}}$ is the average of sensitivity estimates of recharge temperature and $R_{T\text{-BC}}$ is the base-case recharge temperature

S7. Groundwater-Flow Direction

The direction of groundwater flow within the alluvial aquifer was derived from measurements taken between 2011 and 2019 and available through the National Water Information System database (NWIS; U.S. Geological Survey, 2020). The median of all available water-level observation measurements for each well was calculated, and then the median was gridded and contoured using the Python programming language and the matplotlib package. Resulting groundwater contours are illustrated in Fig. S12.

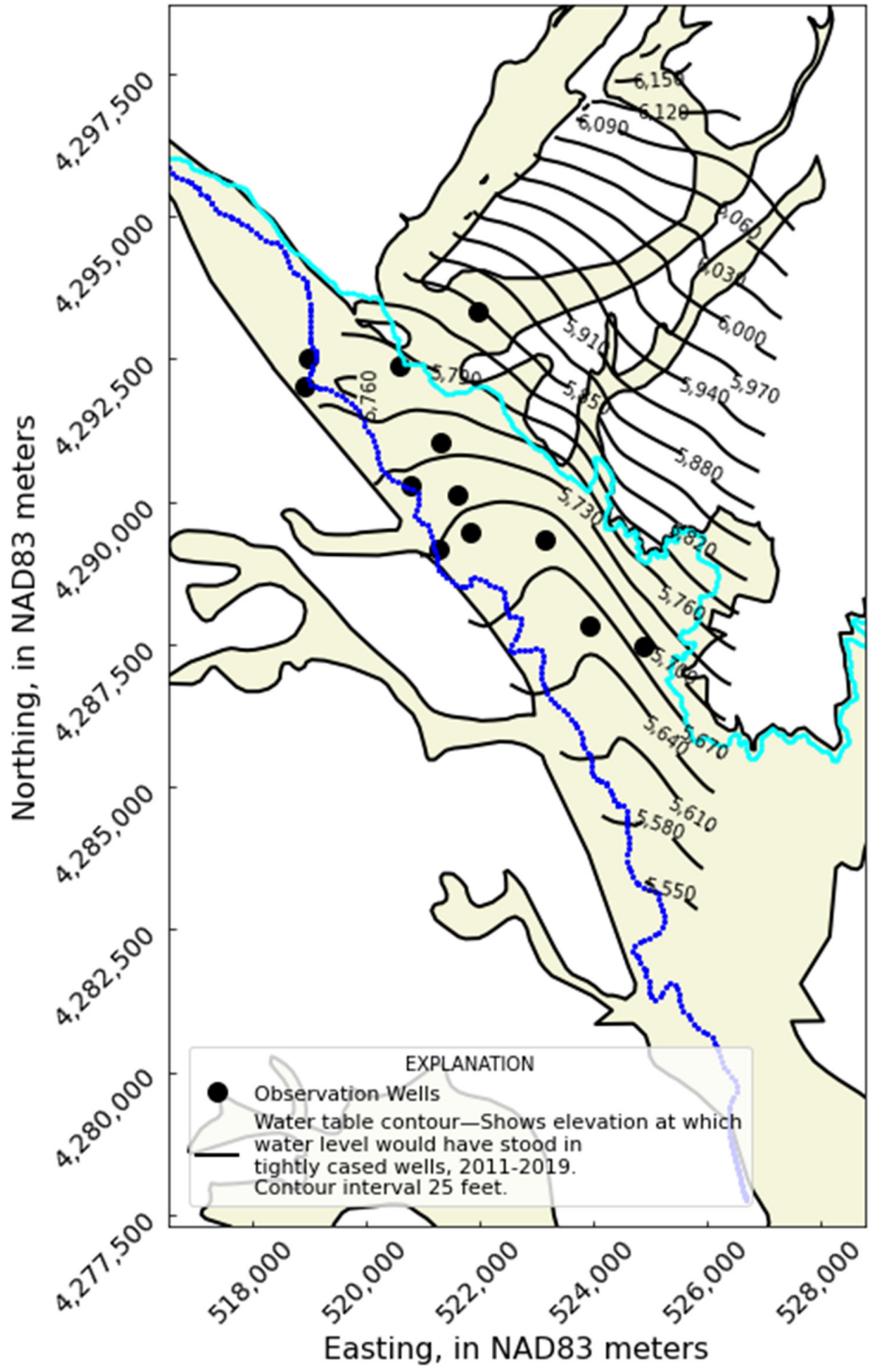

Figure S12 Groundwater-level elevation contours for the Fountain Creek alluvial aquifer. Elevation is in feet above NAVD88.

S8. References

Aeschbach-Hertig, W. and Solomon, D.K., 2013, Noble gas thermometry in groundwater hydrology, *in* Burnard, P., ed., The Noble Gases as Geochemical Tracers: Berlin, Springer-Verlag, p. 81-122.

Alcalá, F.J. and Custodio, E., 2008, Using the Cl/Br ratio as a tracer to identify the origin of salinity in aquifers in Spain and Portugal: Journal of Hydrology, v. 359, p. 189-207, DOI: 10.1016/j.jhydrol.2008.06.028.

Bern, C.R., Walton-Day, K., and Naftz, D.L., 2019, Improved enrichment factor calculations through principal component analysis: Examples from soils near breccia pipe uranium mines, Arizona, USA: Environmental Pollution, v. 248, p. 90-100, DOI: 10.1016/j.envpol.2019.01.122.

Cey, B.D., Hudson, G.B., Moran, J.E., and Scanlon, B.R., 2009, Evaluation of noble gas recharge temperatures in a shallow unconfined aquifer: Groundwater, v. 47, no. 5, p. 646-659, DOI: 10.1111/j.1745-6584.2009.00562.x.

Chapelle, F.H., Bradley, P.M., Thomas, M.A., and McMahon, P.B., 2009, Distinguishing iron-reducing from sulfate reducing conditions in ground-water systems: Groundwater, v. 47, no. 2, p. 300-305.

Davis, S.N., Whittemore, D.O., and Fabryka-Martin, J., 1998 Uses of chloride/bromide ratios in studies of potable water: Ground Water, v. 36, p. 338–350.

Göb, S., Loges, A., Nolde, N., Bau, M., Jacob, D.E., and Markl, G., 2013, Major and trace element compositions (including REE) of mineral, thermal, mine and surface waters in SW Germany and implications for water–rock interaction: Applied Geochemistry, v. 33, p. 127-152, DOI: 10.1016/j.apgeochem.2013.02.006.

Jasechko, S., 2016, Partitioning young and old groundwater with geochemical tracers: Chemical Geology, v. 427, p. 35-42, DOI: 10.1016/j.chemgeo.2016.02.012.

Jasechko, S. and Taylor, R.G., 2015, Intensive rainfall recharges tropical groundwaters: Environmental Research Letters, v. 10, DOI: 10.1088/1748-9326/10/12/124015.

Jung, M. and Aeschbach, W., 2018, A new software tool for the analysis of noble gas data sets from (ground)water: Environmental Modeling and Software, v. 103, p. 120-130, DOI: 10.1016/j.envsoft.2018.02.004.

Jurgens, B.C., McMahon, P.B., Chapelle, F.H., and Eberts, S.M., 2009, An Excel® workbook for identifying redox processes in ground water: U.S. Geological Survey Open-File Report 2009–1004 8 p.

Jurgens, B.C., 2018, Data for Tritium deposition in precipitation in the United States, 1953 - 2012: U.S. Geological Survey data release, https://doi.org/10.5066/P92CEFXN.

Kulongoski, J.T., Hilton, D.R., Cresswell, R.G., Hostetler, S., and Jacobson, G., 2008, Helium-4 characteristics of groundwaters from Central Australia: Comparative chronology with chlorine-36 and carbon-14 dating techniques: Journal of Hydrology, v. 348, p. 176-194, DOI: 10.1016/j.jhydrol.2007.09.048.

Leybourne, M.I. and Johannesson, K.H., 2008, Rare earth elements (REE) and yttrium in stream waters, stream sediments, and Fe–Mn oxyhydroxides: Fractionation, speciation, and controls over REE +

Y patterns in the surface environment: Geochimica et Cosmochimica Acta, v. 72, no. 24, p. 5962-5983, DOI: 10.1016/j.gca.2008.09.022.

Lindsey, B.D., Jurgens, B.C., and Belitz, K., 2019, Tritium as an indicator of modern, mixed, and premodern groundwater age: U.S. Geological Survey Scientific Investigations Report 2019–5090, 18 p., https://doi.org/10.3133/sir20195090.

Mahara, Y., Ohta, T., Morikawa, N., Nakano, T., Tokumasu, M., Hukutani, S., Tokunaga, T., and Igarashi, T., 2014, Effects of terrigenic He components on tritium–helium dating: A case study of shallow groundwater in the Saijo Basin: Applied Geochemistry, v. 50, p. 142-149, DOI: 10.1016/j.apgeochem.2014.02.013.

Mau, D.P., Stogner, R.W., Sr., and Edelmann, P., 2007, Characterization of stormflows and wastewater treatment-plant effluent discharges on water quality, suspended sediment, and stream morphology for Fountain and Monument Creek watersheds, Colorado, 1981–2006: U.S. Geological Survey Scientific Investigations Report 2007–5104, 76 p.

McArthur, J.M., Sikdar, P.K., Hoque, M.A. and Ghosal, U., 2012, Waste-water impacts on groundwater: Cl/Br ratios and implications for arsenic pollution of groundwater in the Bengal Basin and Red River Basin, Vietnam: Science of the Total Environment, v. 437, p. 390-402, DOI: 10.1016/j.scitotenv.2012.07.068.

McMahon, P.B., and Chapelle, F.H., 2008, Redox processes and water quality of selected principal aquifer systems: Groundwater, v. 46, no. 2, p. 259–271.

McMahon, P.B., Lindsey, B.D., Conlon, M.D., Hunt, A.G., Belitz, K., Jurgens, B.C., and Varela, B.A., 2019, Hydrocarbons in upland groundwater, Marcellus Shale Region, northeastern Pennsylvania and southern New York, U.S.A.: Environmental Science and Technology, v. 53, no. 14 p. 8027-8035, DOI: 10.1021/acs.est.9b01440.

Michel, R.L., Jurgens, B.C., and Young, M.B., 2018, Tritium deposition in precipitation in the United States, 1953–2012: U.S. Geological Survey Scientific Investigations Report 2018–5086, 11 p., https://doi.org/10.3133/sir20185086.

Mullaney, J.R., Lorenz, D.L., Arntson, A.D., 2009, Chloride in groundwater and surface water in areas underlain by the glacial aquifer system, northern United States: U.S. Geological Survey Scientific Investigations Report 2009–5086, 41 p.

Noack, C.W., Dzombak, D.A., and Karamalidis, A.K., 2014, Rare earth element distributions and trends in natural waters with a focus on groundwater: Environmental Science and Technology, v. 48, p. 4317-4326, DOI: 10.1021/es4053895.

Peeters, F., Beyerle, U., Aeschbach-Hertig, W., Holocher, J., Brennwald, M.S., and Kipfer, R., 2002, Improving noble gas based paleoclimate reconstruction and groundwater dating using $^{20}Ne/^{22}Ne$ ratios: Geochimica et Cosmochimica Acta, v. 67, no. 4, p. 587–600, DOI: 10.1016/S0016-7037(02)00969-9.

Piper, A.M., 1944, A graphic procedure in the geochemical interpretation of water-analyses: EOS Trans. Am. Geophys. Union, 25 (6), pp. 914-928, doi:10.1029/TR025i006p00914.

Porcelli, D. and Ballentine, C.J., 2002, Models for distribution of terrestrial noble gases and evolution of the atmosphere, *in* Porcelli, D., Ballentine, C.J., and Wieler, R., eds., Noble Gases in

Geochemistry and Cosmochemistry: Quebec, Mineralogical Association of Canada, p. 411-480, DOI: 10.2138/rmg.2002.47.11.

Sun, T., Hall, C.M., and Castro, M.C., 2010, Statistical properties of groundwater noble gas paleoclimate models: Are they robust and unbiased estimators?: Geochemistry, Geophysics, Geosystems, v. 11, no. 2, 18 p., DOI: 10.1029/2009GC002717.

U.S. Geological Survey, 2020, USGS water data for the Nation: U.S. Geological Survey National Water Information System database at https://doi.org/10.5066/F7P55KJN.